

Contrastive Self-supervised Neural Architecture Search

Nam Nguyen, *Student Member, IEEE*, J. Morris Chang, *Senior Member, IEEE*

Abstract—This paper proposes a novel contrastive self-supervised neural architecture search algorithm (NAS), which completely alleviates the expensive costs of data labeling inherited from supervised learning. Our algorithm capitalizes on the effectiveness of self-supervised learning for image representations, which is an increasingly crucial topic of computer vision. First, using only a small amount of unlabeled train data under contrastive self-supervised learning allow us to search on a more extensive search space, discovering better neural architectures without surging the computational resources. Second, we entirely relieve the cost for labeled data (by contrastive loss) in the search stage without compromising architectures’ final performance in the evaluation phase. Finally, we tackle the inherent discrete search space of the NAS problem by sequential model-based optimization via the tree-parzen estimator (SMBO-TPE), enabling us to significantly reduce the computational expense response surface. An extensive number of experiments empirically show that our search algorithm can achieve state-of-the-art results with better efficiency in data labeling cost, searching time, and accuracy in final validation.

Impact Statement—Although transfer learning has achieved many computer vision tasks, finding a customized neural architecture for a specific dataset is still a promising solution for higher performance. However, the process of searching a neural architecture usually demands extensive computational resources. This paper introduces a neural architecture search algorithm that leverages newly developed contrastive self-supervised learning for image representations. Thus, our proposed approach entirely alleviates the cost of data labeling in the search stage. Moreover, our approach outperforms state-of-the-art NAS algorithms in mainstream datasets regarding predictive performance and computational expense.

Index Terms—Neural architecture search; Self-supervised learning; Sequential model-based optimization.

I. INTRODUCTION

Automated neural search algorithms have significantly enhanced the performance of deep neural networks on computer vision tasks. These algorithms can be categorized into two subgroups: (1) flat search space, where automated methods attempt to fine-tune the choice of kernel size, the width (number of channels) or the depth (number of layers), and (2) (hierarchical) *cell-based search space*, where algorithmic solutions search for more minor components of architectures, called *cells*. A single neural cell of deep neural architectures possesses a complex graph topology, which will be later stacked to form a more extensive network.

Although state-of-the-art NAS algorithms have achieved an increasing number of advances, several problematic factors should be considered. The main issue is that most NAS

algorithms use the accuracy in validation inherited from supervised learning as the selection criteria. It leads to a computationally expensive search stage when it comes to sizable datasets. Hence, recent automated neural search algorithms usually did not search directly on large datasets but instead searching on a smaller dataset (CIFAR-10), then transferring the found architecture to more enormous datasets (ImageNet). Although the performance of transferability is remarkable, it is reasonable to believe that searching directly on source data may drive better neural solutions. Besides, entirely relying on supervised learning requires the cost of data labels. It is not considered a problematic aspect in well-collected datasets, such as CIFAR-10 or ImageNet, where the labeled samples are adequate for studies. However, it may become a considerable obstacle for NAS when dealing with data scarcity scenarios. Take a medical image database as an example, where studies usually cope with expensive data curation, especially involving human experts for labeling. Hence, the remedy for such problems is vital to deal with domain-specific datasets, where the data curation is exceptionally costly. Finally, cell-based NAS algorithms’ time complexity increases when the number of intermediate nodes within cells is ascended in the prior configured search space. Previous works show that searching on larger space brings about better architectures. However, the trade-off between predictive performance and search resources is highly concerned.

We propose an automated cell-based NAS algorithm called Contrastive Self-supervised Neural Architecture Search (CSNAS). Our work’s primary motivation is to offer high-performance neural architectures by expanding the search space without any trade-off of search cost. It is clear that searching larger space potentially increases the chance to discover better solutions. We realize that goal by employing the advances of self-supervised learning, which only requires a small number of samples used for the search stage to learn image representations. Besides, thanks to the nature of self-supervised learning, we entirely relieved the cost for labeled data in the search stage. It is significant to mention since, in many domain-specific computer vision tasks, the unlabeled data is abundant and inexpensive, while labeled samples are typically scarce and costly. Thus, we are now able to use a cost-efficient strategy for neural architecture search. Furthermore, we directly address the natural discrete search space of the NAS problem by SMBO-TPE, which evaluates the costly contrastive loss by computationally inexpensive surrogates. We have been made our implementation for public availability, hoping that there will be more research investigating our algorithm’s efficiency concerning computer vision applications.

Nam Nguyen is with the Electrical Engineering Department, University of South Florida, Tampa, Florida. (e-mail: namnguyen2@usf.edu)

The code for implementation can be found at GitHub repo: "https://github.com/namnguyen0510/CSNAS". Moreover, the detailed hyper-parameter setting is given in Section A and B.

II. RELATED WORK

In this section, we first introduced state-of-the-art supervised neural architecture search in Section II-A. Second, the overview of self-supervised learning will be discussed in Section II-B. We then outline state-of-the-art self-supervised NAS algorithm in Section II-C. Finally, we provide our point-of-view on the merits of NAS algorithms in Section II-D, followed by a highlight to distinguish our CSNAS from other approaches. The summary of contribution will also be given at the end of the section.

A. Supervised Neural Architecture Search

We briefly outline the advantages of state-of-the-art supervised NAS algorithms in this section. The discovered architectures searched by supervised NAS algorithms have established highly competitive benchmarks in both image classification tasks [1]–[4] and object detection [1]. The best state-of-the-art supervised neural architecture search algorithms are extremely computationally expensive despite their remarkable results. A reason for inefficient searching process is lied on the dominant approaches: reinforcement learning [5], evolutionary [4], sequential model-based optimization (SMBO) [3], MCTS [6] and Bayesian optimization [7]. For instance, searching for state-of-the-art models took 2000 GPU days under reinforcement learning framework [5], while evolutionary required 3150 GPU days [4]. Several well-established algorithmic solutions for neural architecture search have overcome expensively computational requirements without the lack of scalability: differentiable architecture search [8]–[10] enables gradient-based search by using continuous relaxation and bilevel optimization; progressive neural architecture search utilized heuristic search to discover the structure of cell's [3]; sharing or inheriting weights across multiple child architectures [11]–[14] and predicting performance or weighting individual architecture [15], [16]. Although these latter approaches can reach state-of-the-art results with efficiency concerning searching time, they may be affected by the inherited issue from gradient-based approaches, which finding the local minimum solutions. Apart from that, most state-of-the-art neural architecture search algorithms require full knowledge of training data. Thus, the searching process is frequently performed on a smaller dataset (e.g., CIFAR-10 or CIFAR-100), then the discovered architecture will be trained on a bigger dataset (e.g., ImageNet) to evaluate the transferability.

Although we can relax the constrain of using the same dataset in the search phase and evaluation phase by transferring the learned architecture, it is reasonable to believe that training with the constrain may result in better solutions.

B. Self-supervised Learning for Learning Image Representation

Self-supervised learning has established extremely remarkable achievements in natural language processing [17]–[19].

Hence learning visual representation has drawn great attention with a large scale of literature that has explored the application of self-supervised learning for video-based and image-based classification. Within the scope of this paper, we only focus on self-supervised learning for an image classification task. Generally, mainstream approaches for learning image representations can be categorized into two classes: generative, where input pixels are generated or modeled [20]–[23]; and discriminative, where networks are trained on a pretext task with a similar loss function. The key idea of discriminative learning for visual representations is the designation of pretext task, which is created by pre-assigned targets and inputs derived from unlabeled data: distortion [24], rotation [25], patches or jigsaws [26], colorization [27]. Moreover, the most recent research interests of self-supervised learning have been drawn from contrastive learning in the input latent space [28]–[32], which promisingly showed comparable achievement to supervised learning. [31]–[33] provide convincing evidence of the capacity to learn image representations of contrastive self-supervised learning, which only require a small proportion of training data (1% to 10%) on linear evaluation to reach supervised learning performance. This work also studied the effect of contrastive self-supervised learning of different backbone architectures, which empirically shows that the predictive performance consistently gains when scaling backbone networks. Moreover, a solid theoretical analysis of self-supervised learning (or self-training) is introduced by [34]. Under simplified but practical assumptions that (1) a subset of low confident samples must expand to a neighborhood with higher confidence concerning the subset and (2) neighborhoods of samples from different classes are minimally overlapped, self-supervised learning on unlabeled data with input-consistency regularization will result in higher accuracy in comparison to labeled data.

C. Self-supervised Learning Neural Architecture Search

First, we would like to give a simplified design for self-supervised NAS algorithms, including two main components: (1) choices of the self-supervised learning method and (2) search strategy. In the current literature, SSNAS [35] and UnNAS [36] also introduced self-supervised NAS algorithms that leverage the DART algorithm for search strategy. Moreover, the choice of the self-supervised learning method of SSNAS is SimCRL, while UnNAS utilized invariant pretext tasks. It is worth mentioning that self-supervised learning based on pretext tasks is distinguishable from contrastive self-supervised learning SimCRL. The former approach assigns pseudo-labels to unlabeled data (rotation angle, colorization type, suffer and solve jigsaw puzzles), then trains neural architecture based on these generated labels under supervised learning using the conventional loss function of supervised learning. To some extent, we still observe supervised learning within self-supervised learning based on pretext tasks since it can be considered as supervised training on pseudo-labels. On the other hand, contrastive self-supervised learning trains neural architectures to maximize the agreement between positive pairs (augmented views from the same instance) while minimizing the agreement between negative pairs (augmented view

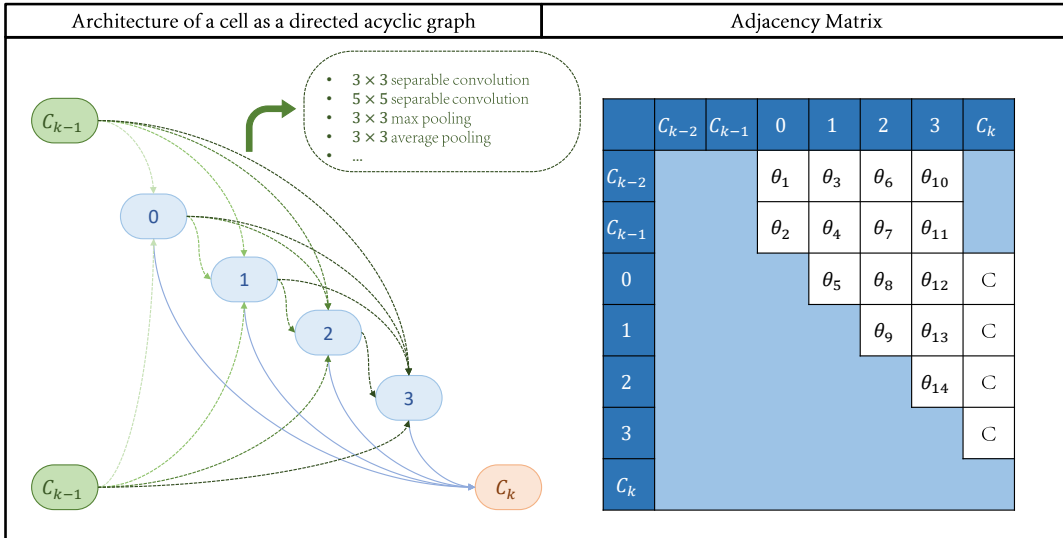


Fig. 1: A graph representation of cell architecture. Left figure: dashed lines represent connections between nodes via a choice of operations; solid lines depict fixed connections. Right figure: the adjacency matrix of the corresponding cell architecture. All shaded entries are zeros since it is impossible to establish corresponding connections. Each θ_i is a random variable representing a choice of operation.

from different instances). Hence, contrastive self-supervised learning eliminates the trait of supervised learning by noise contrastive loss while achieving much better results (very closed to supervised learning) in comparison to pretext task self-supervised learning [31]–[33].

SSNAS is inspired by the fact that all architectures in the search space are over-fitted on the training data. Thus, their selection criteria are based on the architecture’s generalization over the training data. To realize their goal, they used the margin-based search, which involves two splits of training data. Each neural architecture candidate is trained on one split to increase the margin between samples. The selected candidate is the neural architecture maintaining the most significant distance between instances.

On the other hand, UnNAS (from the same author of PNAS [37]) attempted to answer a fascinating question: “Are labels necessary for Neural Architecture Search?”. The work searched neural architecture by DART algorithm using the pretext-task-assigned dataset, including rotation, colorization, and solving a jigsaw puzzle. Both studies provide compelling experimental results showing that self-supervised NAS can search for high-performance neural solutions while relieving the cost of data annotations in the search stage.

D. Merits of NAS algorithms and Contribution of CSNAS

In this section, we will discuss the merits and evaluation criteria for NAS algorithms. First, we would like to quote a well-known aphorism by statistician George Box: “All models are wrong, but some are useful.” This quote is accurate when we assess NAS algorithms since each approach brings about different merits to the research community. Early supervised

NAS algorithms [4], [5] are several of frontiers in supervised NAS algorithms, which successfully searched neural architecture while remaining the constraint of searching data and evaluating data. However, they need to make a massive trade-off with thousands of searching hours. Thus, such an approach’s disadvantage is that it is nearly impossible to implement with limited computational resources. With the growth of research interest from the field, many sub-sequence works successfully reduce the computational requirements while maintaining high predictive power [8], [13], [37], [38]. However, such algorithms still have several weaknesses. For example, DART and sub-sequence approaches such as PC-DART and P-DART result in different cell architectures even though they share the same initial search space. Thus, DART could find a local optimum for the NAS problem. However, we cannot deny that DART offers us the first gradient-based NAS algorithms in accuracy and searching resources.

Moreover, recent work such as SSNAS and UnNAS successfully relieve the cost of labeled data in the search stage while achieves comparable results with supervised NAS. Any supervised NAS algorithm can perform self-supervised NAS if we take the labels for grated in the search stage. Hence, it is not reasonable to compare supervised NAS and self-supervised NAS based on the test accuracy. Intuitively, supervised NAS algorithms should achieve a better predictive performance since they have access to the train set’s full knowledge, which includes data with annotations. However, we are more often than not dealing with computer vision problems involving data scarcity scenarios, in which the cost for data annotations is expensive while unlabeled data are much more abundant. In this case, self-supervised NAS algorithms surpass every supervised NAS algorithm since they can leverage the addi-

tional unlabeled samples, which are entirely take for granted by supervised NAS algorithms. Nevertheless, self-supervised learning NAS also inherits several issues from its backbone training procedure. First, there could be a loss of information while using pretext tasks pseudo-labels or contrastive noise estimators compared to the conventional loss of supervised learning. Recent self-supervised NAS algorithms UnNAS and SSNAS show a minimal gap of such loss on a nicely collected database (CIFAR-10 and ImageNet), including well-represented training samples with equal distribution. However, such loss of information is tough to indicate since it is data-dependent universally. However, we can approximate the loss of information by comparing supervised NAS algorithms and baseline random on a specific database. Second, the time complexity of search under contrastive self-supervised learning is more considerable than supervised learning search since it requires multiple inputs to evaluate the contrastive loss. This issue does not appear in pretext task self-supervised learning from UnNAS since it trains a given neural architecture under supervised learning with pseudo-labels generated by given pretext tasks.

We distinguish our proposed CSNAS from other self-supervised NAS algorithms by two main points. First, we leverage a different contrastive self-supervised learning PIRL [33] for learning image representations within the search phase. SSNAS used SimCRL, which benefits from an extensive training batch size (initially 4096 samples per mini-batch) and a long searching process. Thus, it is a clear obstacle for practical purposes due to its computationally expensive resources. In contrast, by using a memory-bank, PIRL allows self-supervised learning with computationally affordable batch size while remaining the adequate negative samples per mini-batch ($4\times$ smaller compared to SimCRL). Second, it is clear that there will be an increase in the searching time if we directly employ supervised NAS’s search strategy for self-supervised NAS. Hence, we compromise the surge by sequential model-based optimization (SMBO) with a tree-structured Parzen estimator (TPE). Our empirical experiments (Sect IV-B) show that architectures searched by CSNAS on CIFAR-10 outperform hand-crafted architectures [39]–[41] and can achieve high predictive performance in comparison to state-of-the-art NAS algorithms. We also investigate our proposed approach’s domain adaption on a medical imaging database under a data scarcity scenario. The case study provides us a deeper insight into the effectiveness of contrastive learning and gives us a promising result of CSNAS in practice. We summarize our contributions as follows:

- We introduce a novel algorithm for self-supervised neural architecture search, which relieves the expensive cost of data collecting/labeling on the search stage. Our proposed algorithm benefits the data scarcity scenario by leveraging the arising cutting-edges of self-supervised learning for image representations when a small number of unlabeled samples are available.
- Our approach is the first NAS framework based on Tree Parzen Estimator (TPE) [42], which is well-designed for discrete search spaces of cell-based NAS. Moreover,

the prior distribution in TPE is non-parametric densities, which allows us to sample many neural architectures to evaluate the expected improvement for surrogates, which is computationally efficient. Moreover, surrogate models’ usage reduces the expensive cost of true loss function during the search phase. Thus, we can improve search efficiency and accuracy with CSNAS even when the search space is expanded. CSNAS achieves state-of-the-art results with 2.66% and 25.6% test error in CIFAR-10 [43] and ImageNet [44], without any trade-off of search costs.

- We also evaluate the domain adaption ability of our proposed approach on a medical imaging database involving skin lesion classification. Our searched neural architecture on a limited dataset without annotations is well-designed and well-customized for skin lesion classification, which outperforms state-of-the-art architectures under transfer learning, reaching 88.68% of accuracy in the test set. Moreover, the qualitative evaluation shows a shred of solid evidence that neural architecture searched by CSNAS possess a better ability to learn image representations in terms of predictive performance and robustness to noises.

We organize our work as follows: Sect. III mathematically and algorithmically illustrates our proposed approach, while Sect. V-B will give the experimental results and comparison with state-of-the-art NAS on CIFAR-10 and ImageNet. Moreover, we report a detailed analysis of a case study involving skin lesions in Section V. Finally, we will discuss the analysis and future work in Sect. VI.

III. METHODOLOGY

We will generally describe two main fundamental components of our study: neural architecture search and contrastive self-supervised visual representation learning in Sect. III-A and Sect. III-B. Finally, we will formulate the Contrastive Self-supervised Neural Architecture Search (CSNAS) as a hyper-parameters optimization problem and establish its solution by tree-structured Parzen estimator in Sect. III-C

A. Neural Architecture Search

1) *Neural Architecture Construction* : We employ the architecture construction from [1], [5], where searched cell are stacked to form the final convolutional network. Each cell can be represented as a directed acyclic graph of $N + 3$ nodes, which are the feature maps and each corresponding operation $o^{(i,j)}$ forms directed edges (i, j) . Following [1]–[4], we assume that a single cell consists of two inputs (outputs of the two previous layers C_{k-2} and C_{k-1}), one single output node C_k and N intermediate nodes. Latent representations in intermediate nodes are included, which computed as in [8]:

$$\mathbf{x}^{(j)} = \sum_{i < j} o^{(i,j)}(\mathbf{x}^i)$$

The generating set $\mathcal{O} = \{o^{(i,j)}\}$ for operations between nodes is employed from the most selected operators in [1], [4], [5], where includes seven non-zero operations: 3×3

and 5×5 dilated separable convolution, 3×3 and 5×5 separable convolution, 3×3 max pooling and average pooling, identity and zero operation (skip-connection). We retain the same search space as in DARTS [8]. The total number of possible DAGs (without graph isomorphism) containing N intermediate nodes with a set of operators \mathcal{O} are:

$$\prod_{k=1}^N \frac{(k+1)k}{2} \times (|\mathcal{O}|^2).$$

We encode each cell’s structure as a configurable vector θ of length $\sum_{i=2}^{N+1} i$ and simultaneously search for both normal and reduction cells. Therefore the total number of viable cells will be raised to the power of 2. Thus, the cardinality of \mathcal{F} - set of all possible neural architectures - is $(|\mathcal{O}|^{\sum_{i=2}^{N+1} i})^2$. Also, we observed that the discrete search space for each type of cells (normal and reduction) is enormously expanded by a factor of $|\mathcal{O}|^{(N+1)}$ when increasing the number of intermediate nodes from N to $N+1$. Consequently, state-of-the-art NAS can only achieve a low search time (in days) when using $N=4$, while ascending N to 5 usually takes a much longer search time, up to hundreds of days. Our approach treats the high time complexity when expanding the search space by (1) using only a small proportion of data under contrastive learning for visual representations and (2) evaluating the loss by surrogate models, which requires much less computational expense. Details of these methods will be discussed in the next sections.

B. Contrastive Self-supervised Learning

We employ a recent contrastive learning framework in PIRL [33], allowing multiple views on a sample. Let $\mathcal{D} = \{\mathbf{x}_i\}_{i=1}^{|\mathcal{D}|}$ be a train set (for searching) and $\mathcal{F} = \{f_{\theta}(\cdot)\}_{\theta \in \Theta}$ be a set of all neural architecture candidates:

- Each sample $\mathbf{x}_i \in \mathbb{R}^{H \times W \times 3}$ is first taken as input of a stochastic data augmentation module, which results in a set of correlated views $\mathbf{x}_i^t = \{\mathbf{x}_i^{(1)}, \dots, \mathbf{x}_i^{(M)}\}$. Within the scope of this study, three simple image augmentations are applied sequentially for each data sample, including: random/center cropping, random vertical/horizontal flipping and random color distortions to grayscale. The set $\mathcal{X} = \{\mathbf{x}_i\} \cup \{\mathbf{x}_i^t\}$ is called positive pair of sample \mathbf{x}_i .
- Each candidate architecture $f_{\theta}(\cdot)$ is used as a base encoder to extract visual representations from both original sample \mathbf{x}_i and its augmented views \mathbf{x}_i^t . We use the same multilayer perceptron $g(\cdot)$ at the last of all neural candidates, projecting its feature maps of original \mathbf{x}_i image under $f_{\theta}(\cdot)$ into a vector \mathbb{R}^p . For augmented views, another intermediate MLP $l(\cdot) : \mathbb{R}^{M \times p} \rightarrow \mathbb{R}^p$ is applied on concatenation of $\{f_{\theta}(\mathbf{x}_i^{(m)})\}$ for $m \in M$. We denote the representing vectors of original image and augmented views as \mathbf{z}_i and \mathbf{z}_i^t , respectively.

We also use the cosine similarity as the similarity measurement as in [32], [33], yielding $s(\mathbf{u}, \mathbf{v}) = \mathbf{u}^T \mathbf{v} / \|\mathbf{u}\| \cdot \|\mathbf{v}\|$. Each minibatch of K instances is randomly sampled from \mathcal{D} , giving $M \times K$ data points. Similar to [45], a positive pair is corresponding to in-batch negative examples, which are other

$M(K-1)$ augmented samples, forming a set of negative sample \mathcal{X}' . Similarly, each negative samples are extracted visual representations as $\mathbf{z}'_i = g(f_{\theta}(\mathbf{x}'_i))$. Following [33], we compute the noise contrastive estimator (NCE) of a positive pair \mathbf{x}_i and \mathbf{x}_i^t using their corresponding \mathbf{z}_i and \mathbf{z}_i^t , given by

$$\ell(\mathbf{z}_i, \mathbf{z}_i^t) = \frac{\exp(\frac{s(\mathbf{z}_i, \mathbf{z}_i^t)}{\tau})}{\exp(\frac{s(\mathbf{z}_i, \mathbf{z}_i^t)}{\tau}) + \sum_{\mathbf{x}'_i \in \mathcal{X}'} \exp(\frac{s(\mathbf{z}_i, \mathbf{z}'_i)}{\tau})}. \quad (1)$$

The estimators are used to minimize the loss:

$$\mathcal{L}_{\text{NCE}}(\mathbf{x}_i, \mathbf{x}_i^t) = -\log \ell(\mathbf{z}_i, \mathbf{z}_i^t) - \sum_{\mathbf{x}'_i \in \mathcal{X}'} \log [1 - \ell(\mathbf{z}_i, \mathbf{z}'_i)] \quad (2)$$

The NCE loss maximizes the agreement between the visual representation of the original image \mathbf{x}_i and its augmented views \mathbf{x}_i^t , together with minimizes the agreement between \mathbf{x}_i and \mathbf{x}'_i . We use memory-bank approach in [33], [46] to cache the representations of all samples in \mathcal{D} . The representation \mathbf{r}_x in memory-bank \mathcal{M} is the exponential moving average of \mathbf{z}_i from prior epochs. The final objective function for each neural candidate is a convex function of two losses as in Equation 2:

$$\mathcal{L}_{\theta}(\mathbf{x}, \mathbf{x}^t) = \lambda \mathcal{L}_{\text{NCE}}(\mathbf{r}_x, \mathbf{z}^t) + (1 - \lambda) \mathcal{L}_{\text{NCE}}(\mathbf{r}_x, \mathbf{z}) \quad (3)$$

Finally, these loss values establish the scoring criteria for neural architectures under sequential model-based optimization, which will be discussed in the next section.

C. Tree-structured Parzen Estimator

As mentioned in the previous sections, we aim to search on a larger space in order to discover a better neural solutions. Nevertheless, the main difficulty when expanding the search space due to the exponential surge in the time complexity. Thus, we are motivated to study an optimization strategy that might reduce the computational cost. We employ the sequential model-based optimization (SMBO), which has been widely used when the fitness evaluation is expensive. This optimization algorithm can be a promising approach for cell-based neural architecture search, since current state-of-the-art NAS algorithms use the loss in validation as the fitness function, which is computational expensive. The evaluation time for each neural candidate tremendously surges when the number of training samples or sample’s resolution increases. In the current literature, PNAS [3] is the first framework which apply SMBO for cell-based neural architecture search. The surrogate model of in PNAS is used to predict the performance of neural architectures without training them. In contrast to their approach, where the fitness function is in-validation accuracy, we model the contrastive loss in Equation 3 by a surrogate function $S(\cdot)$, which requires less computational expenses. Specifically, a large number of candidates will be drawn to evaluate the expected improvement at each iteration. The surrogate function approximated the contrastive loss over the set of drawn points, resulting in cheaper computational cost. Mathematically, the optimization problem is formulated as

$$\theta^* = \arg \min_{\theta \in \Theta} \mathcal{L}_{\theta}(\mathbf{x}, \mathbf{x}^t)$$

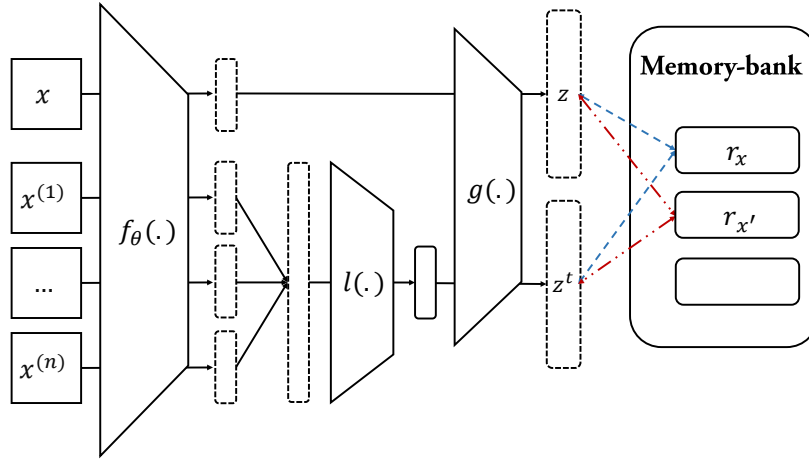


Fig. 2: PIRL genetic framework: Contrastive learning maximizes the similarity between the image representation of original image x and its augmented views with its visual presentations r_x in the memory-bank (dashed green line), while the agreement with negative samples r'_x is minimized (dashed-dotted red line).

Algorithm 1 Sequential Model-Based Algorithm [42]

Given $(\mathcal{L}_{\theta^*}, M_0, I, S)$:

- 1) **Initialize** history $\mathcal{H} \leftarrow \emptyset$
 - 2) **For** iteration $i = 1$ **to** I :
 - $\theta^* \leftarrow \arg \min_{\theta} S(\theta, M_{i-1})$
 - Evaluate $\mathcal{L}_{\theta^*}(x, x^t)$
 - Update $\mathcal{H} \leftarrow \mathcal{H} \cup (\theta^*, \mathcal{L}_{\theta^*}(x, x^t))$
 - Fit M_i to \mathcal{H}
 - 3) **Return** \mathcal{H}
-

The SMBO algorithm is summarized in Algorithm 1, which attempts to optimize the Expected Improvement (EI) criterion [42]. Given a threshold value t^* , EI is the expectation under an arbitrary model M , that $\mathcal{L}_{\theta}(x, x^t)$ will exceed t^* . Mathematically, we have:

$$\text{EI}_{t^*} := \int_{-\infty}^{\infty} \max(t^* - t, 0) p_M(t|\theta) dt. \quad (4)$$

While Gaussian-process approach models $p(t|\theta)$, the tree-structured Parzen estimator (TPE) models $p(\theta|t)$ and $p(t)$, the it decomposes $p(\theta|t)$ to two density functions:

$$p(\theta|t) = \begin{cases} l(\theta) & \text{if } t < t^* \\ g(\theta) & \text{if } t \geq t^* \end{cases}, \quad (5)$$

where $l(\theta)$ is the density function of candidate architectures corresponding to $\{\theta^{(i)}\}$, such that $\mathcal{L}_{\theta^{(i)}}(x, x^t) < t^*$ and $g(\theta)$ is formed by the remaining architectures. As a result, the EI in Equation 4 is reformed as:

$$\begin{aligned} \text{EI}_{t^*}(\theta) &= \int_{-\infty}^{t^*} (t^* - t) p(t|\theta) dt \\ &= \int_{-\infty}^{t^*} (t^* - t) \frac{p(\theta|t)p(t)}{p(\theta)} dt \propto \left(\gamma + \frac{g(\theta)}{l(\theta)} (1 - \gamma) \right)^{-1}, \quad (6) \end{aligned}$$

where γ denotes $p(t < t^*)$. The tree structure in TPE allows us to draw multiple candidates according to $l(\cdot)$ and then evaluate them based on $g(\theta)/l(\theta)$.

IV. EXPERIMENTAL RESULTS ON CIFAR-10 AND IMAGENET

Our experiments on each dataset include two phases, neural architecture search (Sect IV-A) and architecture evaluation (Sect IV-B). In the search phase, we used only 10% of unlabeled data (5,000 samples from CIFAR-10 [43] and approximately 12,000 samples from ImageNet [47]) to search for neural architectures having the lowest contrastive loss mentioned in Equation 3 by CSNAS. The best architecture is scaled to a larger architecture in the validation phase, then trained from scratch on the train set and evaluated on a separate test set.

A. Architecture Search for Convolution Cells

We initialize our search space by the operation generating set \mathcal{O} as in Sect III-A1, which has been obtained by the most frequently chosen operators in [1], [3], [4], [8]. Each convolutional cell includes two inputs C_{k-2} and C_{k-1} (feature maps of two previous layers), a single concatenated output C_k and N intermediate nodes.

We create two searching spaces for CIFAR-10, denoted as CSNAS $_{N=4}$ and CSNAS $_{N=5}$, which are corresponding to the number of intermediate nodes N . With $N = 4$, a configurable vector θ representing a neural architecture have the length of 28 ($\theta_{\text{normal}} = \theta_{\text{reduced}} = 14$), resulting in a search space of size $(8^{14})^2 \approx 2 \times 10^{25}$. We expand our search space by adding a single intermediate node, in the hope of finding a better architecture. $N = 5$ is corresponding to configurable vector θ of length 40, which tremendously surges the total number of possible architectures to 10^{36} . Experiments involved ImageNet only use the latter search space with $N = 5$.

We configure our contrastive self-supervised learning by two augmented views ($M = 2$) for each sample with methods mentioned in Sect. III-B, producing $2 \times (K - 1)$ negative examples for each data instance in a minibatch of size K . We also investigate the effect of M on the search efficiency, which we will discuss in detail in Sect. B. The other two hyper-parameters τ and λ in Equation 1 and Equation 2 are taken

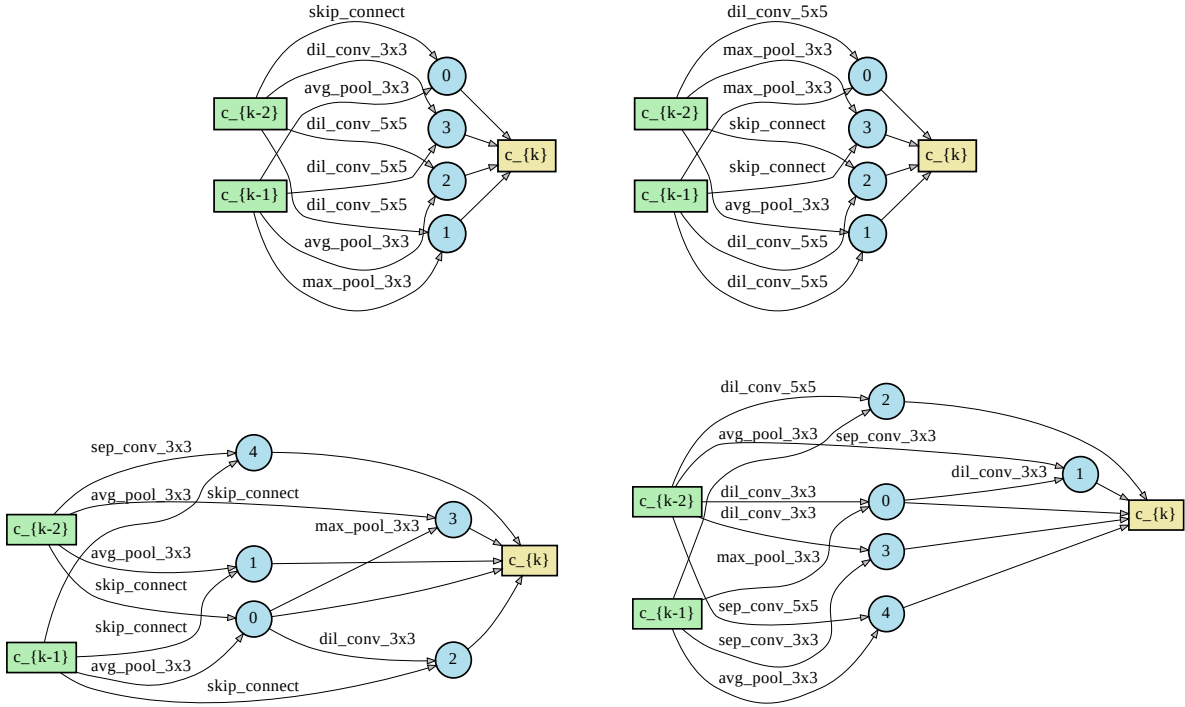


Fig. 3: Cell architecture of $\text{CSNAS}_{N=4}$ and $\text{CSNAS}_{N=5}$ searched on CIFAR-10. Each candidate cell’s architecture is encoded to a vector θ of length 28 ($\theta_{\text{normal}} = \theta_{\text{reduced}} = 14$) when $N = 4$. The length encoded vector increases to 40 when we searched on the configuration space according to $N = 5$. Moreover, two inputs for every intermediate nodes are the feature maps produced by corresponding operations (edges). Produced feature maps will be concatenated at the end of a cell to creating input for sub-sequence cells.

from the best experiment in [33], where $\tau = 0.07$ and $\lambda = 0.5$. Besides, MLPs $g(\cdot)$ and $l(\cdot)$ project encoded convolutional maps to a vector of size $p = 128$. Although we expected a minor impact of the above hyper-parameters, we will leave this tuning problem for further study.

We initialize the same prior density for each component of θ , which is that all operations have the same chance to be picked up at a random trail. 20 random samplings start TPE, then $20K$ sample points are suggested to compute the expected improvement in each subsequent trial. We select only 20% of best-sampled points having the greatest expected improvement to estimate next θ . We also observed that the number of starting trials is insensitive to the searching results while increasing the number of sampling points for computing expected improvement and lowering their chosen percentage ameliorate the searching performance (lower the overall contrastive loss).

We summarize the parameter settings for all experiments in Sect A.

B. Quantitative Evaluation

We select the architecture having the best score from the searching phase and scale it for the validation phase. Within this paper’s scope, we only scale the searched architecture to the same size as baseline models in the literature ($\approx 3M$). All weights learned from the searching phase had been discarded

before the validation phase, where the chosen architecture is trained from scratch with random weights.

Before analyzing the experimental results of CSNAS, we would like to outline several evaluation metrics for a NAS algorithm briefly. To begin with, we emphasize that predictive performance is a sufficient condition for good NAS algorithms. However, it is mandatory further to consider the versatility of NAS algorithms in different scenario. As mentioned in Section II-D, supervised NAS algorithms likely result in better neural architectures than self-supervised learning NAS since they leverage full knowledge of training data (with annotations). On the other hand, self-supervised NAS offers us the opportunity to utilize additional unlabeled out-of-training samples, potentially lifting the curse of data when it comes to a scarcity scenario. Another evaluation metric for NAS algorithms is based on their ability to implement with limited computational resources. Finally, reported results from NAS algorithms are sensitive to the hyper-parameters setting of *evaluation phase*, which may be attributed to the gain in overall performance. For example, DART used the same hyper-parameter setting (or reproduce other NAS with the same setting) with [1], [3], [4], [13]; thus, the gain in accuracy can be entirely attributed to the effectiveness of search strategies. On the other hand, P-DART and PC-DART used a slightly higher regularization (increment of 0.1 drop path probability) and larger batch size while remained the same learning rate

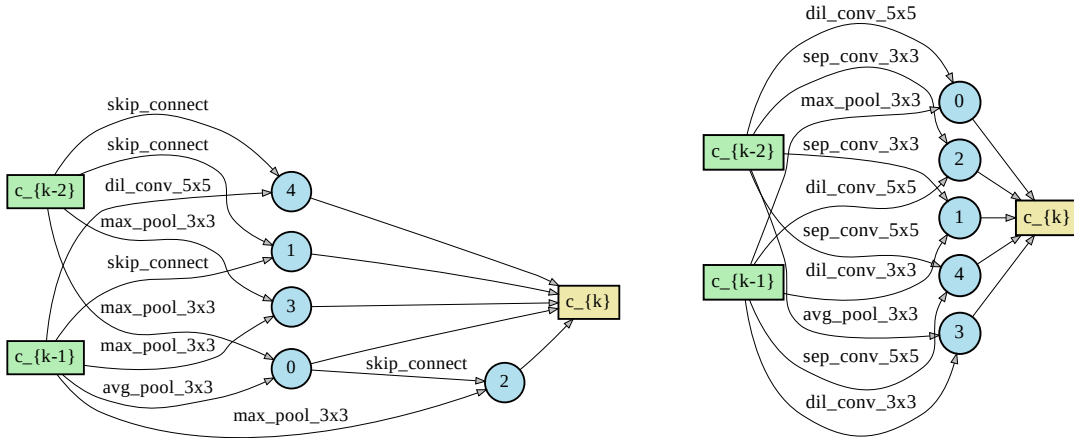


Fig. 4: Cell architecture of $\text{CSNAS}_{N=5}$ searched on ImageNet-1%. The vector θ representing each neural candidate is of length 20.

as DART. The overall improvement may be slightly gained by such random effects in the evaluation phase. However, it cannot be denied that P-DART and PC-DART offer us very highly efficient gradient-based NAS algorithms, tremendously reducing the computational expense in the search phase.

In the first block of Table I, we compare our search with neural architectures designed manually. Searched CSNAS gains approximately 2% and in test accuracy when comparing to ResNet-1001, while smaller gap (about 1%) on comparison to DenseNet-BC and VGG11B. We consider the results from manual designs a baseline for evaluating NAS algorithms since NAS’s motivation is to search for better neural solutions automatically.

In the second block, we report the results from SOTA supervised NAS algorithms. We perform the evaluation phase for CSNAS based on the exact setting used in [3]–[5], [8], [13] to draw fair comparison with these supervised NAS algorithms. Regarding CIFAR-10, we report the performance of architecture searched by CSNAS in Table I. It is highlighted that $\text{CSNAS}_{N=4}$ achieved a slightly better result than DARTS with $16\times$ faster (0.25 in comparison to 4), even though these algorithms share the same search space complexity. Moreover, $\text{CSNAS}_{N=5}$ can reach comparable results with AmoebaNet and NASNet in a tremendously less computational expense (1 vs. 3150 and 2000, respectively). Similarly, the results of CSNAS on ImageNet are reported in Table II. Instead of transferring architecture from CIFAR-10, we directly search for the best architecture using 10% of unlabeled samples from ImageNet (list of the images can be found in [32]). The performance of the network found by CSNAS appears to outperform DART and NASNET-A but to be slightly lower than AmoebaNet-C. Moreover, from both Table I and II, the overall observation is that CSNAS possesses the ability to search for high-performance neural architectures, reaching comparable results with supervised NAS algorithms while using limited knowledge of data in search.

The third block reports the performance of self-supervised

NAS algorithms, including SSNAS and UnNAS-DART. It is noted that the two algorithms and our CSNAS search without using any data annotations. However, both SSNAS and UnNAS-DART used the whole training data (neglecting labels) for search, while we only used a small proportion of original training data. In the experiment on CIFAR-10, our CSNAS reaching slightly lower predictive performance than SSNAS. Regarding ImageNet, our CSNAS obtains a gain of 2% in accuracy compared to SSNAS, while being outperformed by UnNAS-DART with the same gap. The results indicate a loss of information from our CSNAS since we used a small proportion of data without annotations. However, this loss can be considered marginally small concerning the amount of knowledge used. We also conduct a further ablation study in Section IV-D investigating the effect of the amount of data used on the overall performance.

We report the hyper-parameter setting for evaluation phase in Section B.

C. Qualitative Evaluation

We assess the potency of learning visual representations by investigating classification activation maps (CAM) from CSNAS compared to DARTS and PDARTS. In particular, CAM enables well-trained neural architectures to perform multi-computer-vision-task, which includes classification and localization. The heatmap represented in CAM is the class-specific region in an image that primarily influences CNN’s prediction. Moreover, we only consider NAS algorithms with official pre-trained networks for the qualitative evaluation since reproducing such NAS algorithms may breed differences to original results. In the meantime of this study, we only find DARTS and PDARTS offer the pre-trained weights for their derived networks, so we only consider these supervised NAS for further investigation. It is worth mentioning that we do not aim to compare NAS algorithms’ performance based on these heat maps. The qualitative impression is instead used for illustration of CSNAS’s robustness in visual

TABLE I: The performance (in term of test error) of state-of-the-art NAS algorithms on CIFAR-10. The search cost includes only searching time by SMBO-TPE algorithm, excluding the final architecture evaluation cost (See B).

Neural Architecture	Test Error (%)	Params (M)	Search Cost (GPU days)	# Ops	Search Strategy
DenseNet-BC [39]	3.46	25.6	-	-	Manual
VGG11B (2×) [40]	3.60	42.0	-	-	Manual
ResNet-1001 [41]	4.62	10.2	-	-	Manual
AmoebaNet-A + cutout [4]	3.12	3.1	3150	19	Evolution
AmoebaNet-B + cutout [4]	2.55 ± 0.05	2.8	3150	19	Evolution
CARS-I [48]	2.62	3.6	0.4	7	Evolution
Hierarchical evolution [4]	3.75 ± 0.12	15.7	300	6	Evolution
LEMONADE [49]	3.05	4.7	80	-	Evolution
NSGANet [50]	3.85	3.3	8	7	Evolution
BlockQNN [51]	3.54	39.8	96	8	RL
ENAS [13] + cutout	2.89	4.6	0.5	6	RL
NASNet-A [1] + cutout	2.65	3.3	2000	13	RL
BayesNAS [52] + cutout	2.81 ± 0.04	3.4	0.2	-	Gradient-based
DARTS (1 st order) [8] + cutout	3.00 ± 0.14	3.3	1.5	7	Gradient-based
DARTS (2 nd order) [8] + cutout	2.76 ± 0.09	3.3	4	7	Gradient-based
GDAS [53] + cutout	2.93	3.4	0.21	7	gradient-based
P-DARTS [37] + cutout	2.50	3.4	0.2	7	Gradient-based
PC-DARTS [9] + cutout	2.57 ± 0.07	3.6	0.1	7	Gradient-based
ProxylessNAS [54] +cutout	2.08	5.7	4.0	-	Gradient-based
MiLeNAS [55]	2.51 ± 0.11	3.87	0.3	-	Gradient-based
SNAS (moderate) [38] + cutout	2.85 ± 0.02	2.8	1.5	7	Gradient-based
GP-NAS [56]	3.79	3.90	0.9	7	Gaussian-Process-based
PNAS [3]	3.41 ± ±0.09	3.2	225	8	SMBO
SSNAS [35]	2.61	-	0.21	-	Gradient-based
CSNAS _{N=4} (ours) + cutout †	2.71 ± 0.11	3.5	0.25	7	SMBO-TPE
CSNAS _{N=5} (ours) + cutout †	2.66 ± 0.07	3.4	1	7	SMBO-TPE

† Results based on 10 independent runs.

representation learning. Figure 5 shows ten random samples from ImageNet with their CAMs from CSNAS and their competitors. As we can see, the CAMs from CSNAS focus on the correct region-of-interest (ROIs), which means its searched neural architecture makes a prediction based on accurate class-specific regions. Noticeably, the thresholded ROIs with a progressive threshold $\tau = 0.7$ from CSNAS (yellow boxes) are relatively equivalent to PDART, while there are minor differences compared to DART’s ROIs. Thus, it indicates that neural architecture searched by CSNAS can effectively learn visual representations, even when it is explored with limited knowledge from training data. We also observed a consistent result from the case study of skin lesion data (Section V-C), in which the search phase uses entirely out-of-training data.

D. Ablation Study

We further analyse the effectiveness of contrastive learning on neural architecture search and the effectiveness of SMBO-TPE in comparison to random search. The result is summarized in Figure 6. Within this cope of the study, we only use CIFAR-10 for illustration of the analysis. First, we study the impact of the amount of unlabelled data on the performance of CSNAS by extending the search using SMBO-TPE under contrastive self-supervised learning with 100% of the dataset. The first observation is that we need to make a significant trade-off between the accuracy gain and search resources. The searching time using 100% of CIFAR-10 samples surges to 90h on 3GPU (11.25GPU days) while the improvement in accuracy is very

minimal - about 0.04%. In comparison with SSNAS where also used the same number of samples for search, our CSNAS reach a compatible result while using different contrastive learning method and search strategy. On the other hand, we observe a slight loss of information while search without labels under self-supervised learning. Particularly, supervised NAS algorithms possess a slightly better performance than our CSNAS; however, the novelty of ours approach lies on the ability to search without data annotation’s cost. Moreover, the performance gain by using whole dataset is minimal, considering a surge in searching resources. Second, we investigate the effectiveness of contrastive learning by conducting a search using TPE under supervised learning with the same 10% and 100% of data used in CSNAS. Again, the experiment shows that contrastive self-supervised learning induces a loss of information in comparison to supervised learning in 100%. The results based on 10 independent runs show that the mean test error of searching under supervised learning using 100% is 2.56%, 0.08% of improvement. However, searching on a smaller proportion including 10% of data reveals a contrast result, which supervised learning search reaches 2.72% in test error, 0.06% higher than CSNAS. Finally, we study the effect of TPE as search strategy in comparison to random search, which also uses 10% of samples. The random search experiment produces a neural solution with 2.98% in test error, 0.32% larger than neural architecture produced by TPE.

TABLE II: The performance (in term of test error) of state-of-the-art NAS algorithms on ImageNet.

Neural Architecture	Test Err. (%) Top-1 (Top-5)	Params (M)	$\times+$ (M)	Search Cost (GPU days)	Search Strategy
Inception-v1 [57]	30.2(10.1)	6.6	1448	-	Manual
Inception-v2 [58]	25.2(92.2)	11.2	-	-	Manual
MobileNet [59]	29.4(10.5)	4.2	569	-	Manual
ShuffleNet (2 \times)-v1 [60]	26.4(10.2)	\approx 5	524	-	Manual
ShuffleNet (2 \times)-v2 [61]	25.1 (-)	\approx 5	591	-	Manual
NASNet-A [1]	26.0(8.4)	5.3	564	2000	RL
NASNet-B [1]	27.2(8.7)	5.3	488	2000	RL
NASNet-C [1]	27.5(9.0)	4.9	558	2000	RL
AmoebaNet-A [4]	25.5(8.0)	5.1	555	3150	Evolution
AmoebaNet-B [4]	26.0(8.5)	5.3	555	3150	Evolution
AmoebaNet-C [4]	24.3(7.6)	6.4	570	3150	Evolution
AutoSlim [62]	24.6(-)	8.3	532	224	greedy
AtomNAS-A [63]	25.4(7.9)	3.9	258	-	Dynamic network shrinkage
AutoNL-S [64]	22.3(6.3)	5.6	353	32	Single-path
Single-Path [65]	25.0(7.79)	-	-	0.14	Single-path
MnasNet-92 [66]	25.2(8.0)	4.4	388	-	RL
PNAS [3]	25.8(8.1)	5.1	588	255	SMBO
PARSEC [67]	26.0(8.4)	5.6	548	1	SMBO
FBNet-C [68]	25.1(-)	5.5	375	20	SMBO
P-DART [37]	24.1(7.3)	5.4	5.97	2.0	Gradient-based
PC-DART [9]	24.2(7.3)	5.3	597	3.8	Gradient-based
ProxylessNAS [54]	24.9(7.5)	7.1	465	8.3	Gradient-based
MiLeNAS [55]	24.7(7.6)	5.3	584	0.3	Gradient-based
DARTS (2 nd order) [8]	26.7(8.7)	4.7	574	4	Gradient-based
SNAS (mild constraint) [38]	27.3(8.7)	4.3	522	1.5	Gradient-based
RCNet [69]	27.8(9.0)	3.4	294	8	Gradient-based
GDAS [53]	26.0(8.5)	5.3	581	0.8	Gradient-based
SSNAS [35]	27.75(9.55)	-	-	-	Gradient-based
UnNAS-DARTS [36] + Jigsaw	24.1 \pm 0.15(-)	5.2	567	2	Gradient-based
CSNAS _{N=5} (ours) + cutout †	25.8 \pm 0.17(8.3)	5.1	590	2.5	SMBO-TPE

† Results based on 10 independent runs.

V. CASE STUDY

This section investigates the effectiveness of CSNAS on a practical case study, which involves skin lesion classification. The under-investigated problem is an excellent example of a data scarcity scenario, where labeled data is costly (requires expert knowledge), and unlabelled data have zero-cost for annotations. Self-supervised NAS algorithms are suitable for such cases. Moreover, at the same time as our study, CSNAS is the second work considering skin lesion classification. [70] used network morphism to search neural architecture for skin lesion classification. However, they only consider binary classification problems while we performed multi-class classification. We are hoping to compare our CSNAS to other self-supervised NAS. Unfortunately, we cannot find the official implementation of SSNAS and UnNAS in the meantime. It is noted that reproducing the work without official implementation may induce inaccurate observation and false comparison. Therefore, we can only compare our CSNAS to the conventional approach for skin lesion classification, which is transfer learning.

We organize the section as follows: Section V-A summarizes the classification problem with a detailed introduction of the ISIC-2019 database. Section V-B gives a detailed experimental setting for the case study. Finally, we report the quantitative and qualitative results in Section V-C. To avoid confusion with searched architectures from CIFAR-10 and ImageNet, we

named architecture searched on ISIC-2019 as DermoCSNAS.

A. ISIC-2019 Dataset

The dataset of interest is International Skin Imaging Collaboration database (ISIC 2019) ([71]–[73]), which includes a public train set of 25,331 labeled images and a private test set of 8,238 unlabeled images. For the illustration of the proposed neural solution, the unlabeled samples in the test set are used for searching deep neural architecture in a self-supervised manner, and then the found architecture is conventionally trained on the train set to perform classification. It is highlighted that the public train set and private test set provided by ISIC 2019 are not overlapped. The ISIC 2019 public train set originally contains nine classes, which are melanoma (MEL), melanocytic nevus (NV), basal cell carcinoma (BCC), actinic keratosis (AK), benign keratosis (BKL), dermatofibroma (DF), vascular lesion (VASC), squamous cell carcinoma (SCC) and unknown disease (UNK). Since the number of unknown training samples is zero, we only consider defined disease, resulting in a multi-label classification of 8 classes. Table III depicts the distribution of classes and search-train-test-validation splits (follows ratio 80%–5%–15%) for our experiment. Moreover, we also publish the list of train/test/validation samples in the GitHub repository for reproduction purposes.

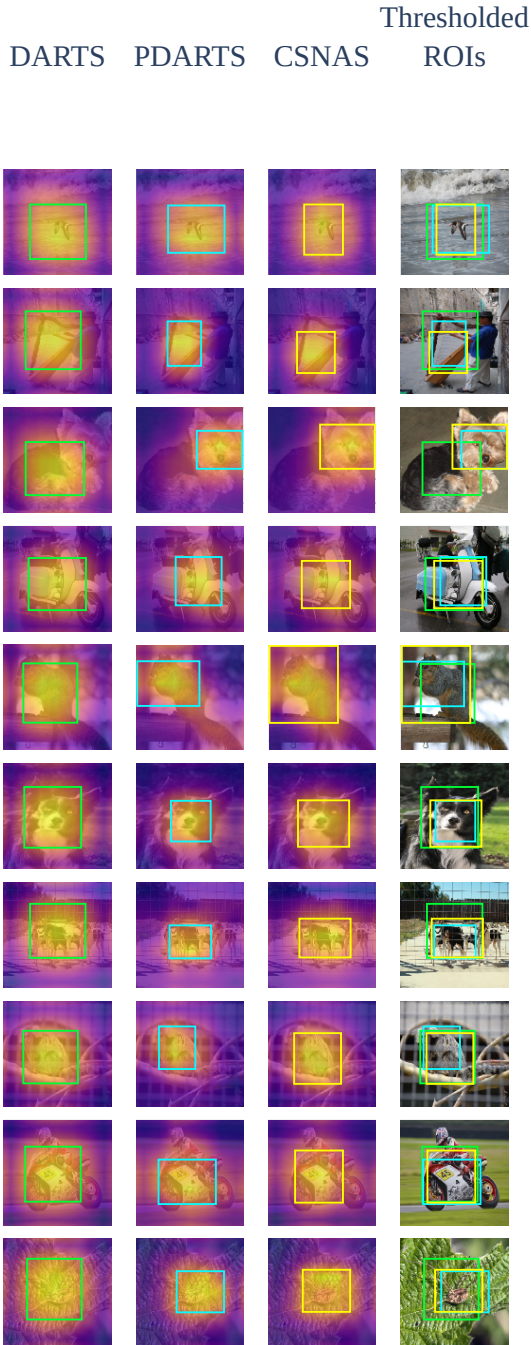


Fig. 5: Qualitative evaluation of CSNAS algorithm. In the first three columns, we represent the Classification Activation Maps (CAM) of ten random samples from DARTS, PDARTS and CSNAS. The last column depicts the thresholded ROIs from CAMs with threshold of $\tau = 0.7$. As we can see from the result, CSNAS can effectively make predictions based on accurate class-specific region within images.

B. Experimental Setup

Our experiment includes two phases, which are (1) searching neural architecture on unlabeled data (ISIC private test set) under a self-supervised learning manner and (2) evaluating discovered neural net on labeled samples (ISIC public train set).

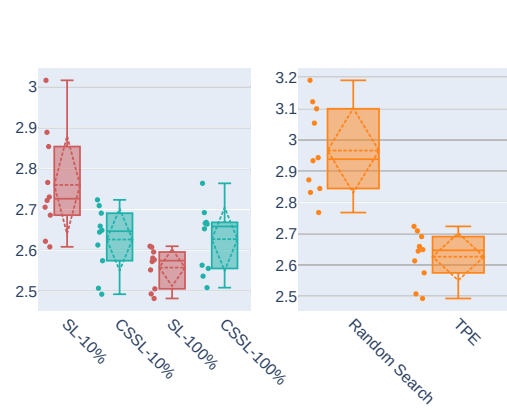


Fig. 6: Effectiveness of contrastive learning and TPE search strategy. The right panel illustrate the comparison between supervised search and self-supervised search. Left panel depicts the comparison between random search and usage of TPE. The set of training parameters is fixed across all experiments (Section B).

TABLE III: ISIC-2019 dataset in detail. The data used for search is out-of-training and accounted for 32.5% of training data.

Dataset	Used Phase	Number of samples	Split
ISIC-2019 private test set	Search	8,238	-
ISIC-2019 public train set	Validation	Train	20,265
		Validation	1,290
		Test	3,776
		Total	25,331
Skin Disease	Annotation	Distribution	
Melanoma	MEL	4,522	17.85%
Melanocytic Nevus	NV	12,875	50.83%
Basal cell carcinoma	BCC	3,323	13.12%
Actinic keratosis	AK	867	3.42%
Benign keratosis	BKL	2,624	10.36%
Dermatofibroma	DF	239	0.94%
Vascular lesion	VASC	253	1%
Squamous cell carcinoma	SCC	628	2.48%
Unknown	UNK	0	0%

To preserve our procedure’s robustness, we wholly removed the learned model weights after the searching phase. Then, we found that neural architecture was trained from scratch using a random initialization in the validation phase.

1) *Search Phase*: Our configuration for this experiment is similar to CIFAR-10 and ImageNet. First, we investigate two configurations for searching spaces, corresponding to $N = 4$ and $N = 5$ intermediate nodes. The architectures found under these settings are denoted as DermoCSNAS-4 and DermoCSNAS-5, in which the encoded vector θ of a neural candidate DermoCSNAS-4 is a 28-dimensional vector, while the corresponding vector for DermoCSNAS-5 is a 40-dimensional vector. As a result, the number of possible neural candidates exponentially increases (5×10^{10} times) when added to only one intermediate node. Second, we generate neural candidates using the operation generating set \mathcal{O} mentioned in section- and perform contrastive self-supervised learning with two augmented views ($M = 2$) for each sample, resulting

TABLE IV: Comparisons between state-of-the-art neural architectures and our proposed model, in terms of test accuracy and model complexity. The results of our DermoCSNAS are mean and variance from 10 independent runs, which use the same set of training hyper-parameters in Section V-B2. Moreover, we use the same experimental setting (data augmentation and training parameters) across all transfer learning experiments in order to provide unbiased results.

Neural Architecture	Params (%) (M)	FLOPS (G)	Test Acc. (%)	Melanoma F1-score
DPN-131 [75]	79.3	16.0	86.23	0.79
EfficientNet-B0 [76]	5.3	0.39	82.14	0.80
ResNet152 [77]	60.0	11.3	84.00	0.75
ResNet101 [77]	44.6	8.0	87.76	0.81
Inception-v4 [57]	46.0	12.3	85.99	0.79
Inception-ResNet-v2 [78]	55.8	11.75	87.53	0.80
NASNet [1]	88.9	24.0	87.80	0.82
PNASNet [3]	86.1	25.2	87.87	0.81
SENet101 [79]	49.2	8.0	87.55	0.81
SENet154 [79]	145.8	42.3	88.00	0.83
Xception [80]	23.0	8.4	87.18	0.80
DermoCSNAS _{N=4}	3.55	0.503	87.94 ± 0.04	0.83
DermoCSNAS _{N=5}	4.15	0.560	88.68 ± 0.02	0.84

in $2 \times (K - 1) = 298$ negative examples for each data point in a mini-batch of $K = 150$ samples. Each candidate contains only 8 layers with 16 initial channels, which is trained using momentum SGD with the learning rate of 0.001 and momentum of 0.9. The hyper-parameter for noise contrastive estimator in Equation is set as $[\tau, \lambda] = [0.07, 0.5]$. Finally, we initialize the TPE by 20 random samplings, followed by $20K$ suggested points for computing the expected improvement of each trial. There only 20% of best candidates having the largest expected improvement is mutated for estimating the next θ . They found neural architecture is illustrated in Figure 7.

2) *Validation Phase*: First, we construct the final neural architecture by expanding the depth (number of layers) and the width (number of initial channels) from the discovered neural cell in the search phase. In both configurations of $N = 4$ and $N = 5$, we stack 18 layers of the founded cell with 48 initial channels since we aim to provide a hardware-aware deep neural architecture, which is restricted under 600 number of multiply-add operation. Noted that all of the reduction cells are in one-half and two-thirds of the depth of model, in which all chosen operations use a stride of 2. Second, we augmented training samples by downsampling to 256×256 before random cropped into 224×224 , then randomly apply horizontal and vertical flipping. Moreover, we prevent over-fitting by linearly increasing path drop out of 0.2 as in ([1], [3]–[5], [8]), cutout of length 16 ([74]) and a small auxiliary classifier (at two-third of model’s depth) with weight of 0.4. Finally, the model is trained with a batch size of 128 using SGD optimizer, which is initialized by 0.02 learning rate and 0.9 weights decay. The learning rate has a decay rate of 0.99 for every 3.5 epoch.

C. Effectiveness analysis

We depict the effectiveness of our approach by comparing it with state-of-the-art models in Table IV. It is noted that other state-of-the-art architectures are fine-tuned with pre-trained weights (transfer learning), while our neural architecture is trained from scratch on the ISIC dataset. Hence it is inevitable

TABLE V: Classification report of our DermoCSNAS_{N=5}. The searched neural architecture possesses high predictive performance. Besides, the precision of Melanoma (cancerous class) is well-established.

Classes	Precision	Recall	F-1 score	Support
Melanoma	0.84	0.81	0.83	647
Melanocytic Nevus	0.92	0.95	0.93	1991
Basal cell carcinoma	0.87	0.90	0.88	465
Actinic Keratosis	0.79	0.62	0.69	119
Benign Keratosis	0.76	0.76	0.76	381
Dermatofibroma	0.85	0.78	0.81	36
Vascular	0.97	0.72	0.82	39
Squamous cell carcinoma	0.75	0.67	0.71	98
Macro average	0.84	0.78	0.81	3776
Weighted average	0.88	0.88	0.88	

that lower-level features in early layers of our model are learned from skin lesion images. In contrast, we need to accept inherited lower-level features from domain datasets (ImageNet or CIFAR-10) once performing transfer learning and fine-tuning pre-trained models. As discussed in the beginning of this section, we cannot reproduce other self-supervised NAS algorithms without significant inaccurate results. Thus, we instead evaluate the performance of DermoCSNAS by comparing to the most conventional approach of skin lesions classification, which is transfer learning. Within the scope of this study, we compare our discovered neural architecture with state-of-the-art deep convolution networks, which include Efficient-B0 ([76]), ResNes-101 and ResNet-152 ([77]), Inception-v4 ([57]), Inception-ResNet-v2 ([78]), DPN-131 ([75]), Xception ([80]), SENet101 and SENet 154 ([79]), NASNet [1], PNASNet [3].

First, the searched neural architecture under the best setting (DermoCSNAS_{N=5}) outperforms other human-crafted model, gaining 0.68% – 4.68% (in compare to SENet154 and ResNet152, respectively). We also observed no trade-off between the model complexity and the overall performance since our model possesses the smallest number of parameters and the number of multiply-add operations. Second, our deep neural architecture is more robust to artifacts (such as badges, human hairs, ink marks). We examine the CAMs extracted from investigated models to determine the most influential region that affects prediction. Figure 8 shows that our customized architecture makes inferences based on skin lesions, together with neglecting noises. Meanwhile, other architectures show the same pattern of error when making the prediction based on these artifacts. Although PNASNet-5-Large can also neglect noises, the heat map is not concentrated on lesion regions as DermoCSNAS. Last but not least, our model has the best F-1 score from malignant classes (Melanoma) at 0.84, while others are ranging from 0.75 to 0.83. It is crucial since our neural intelligence makes no trade-off between the overall accuracy and the balance of precision and recall from cancerous class. The detailed classification report is showed in Table V.

VI. CONCLUSION

We have introduced CSNAS, an automated neural architecture search that completely alleviates the expensive cost of data labeling. Furthermore, CSNAS performs searching on

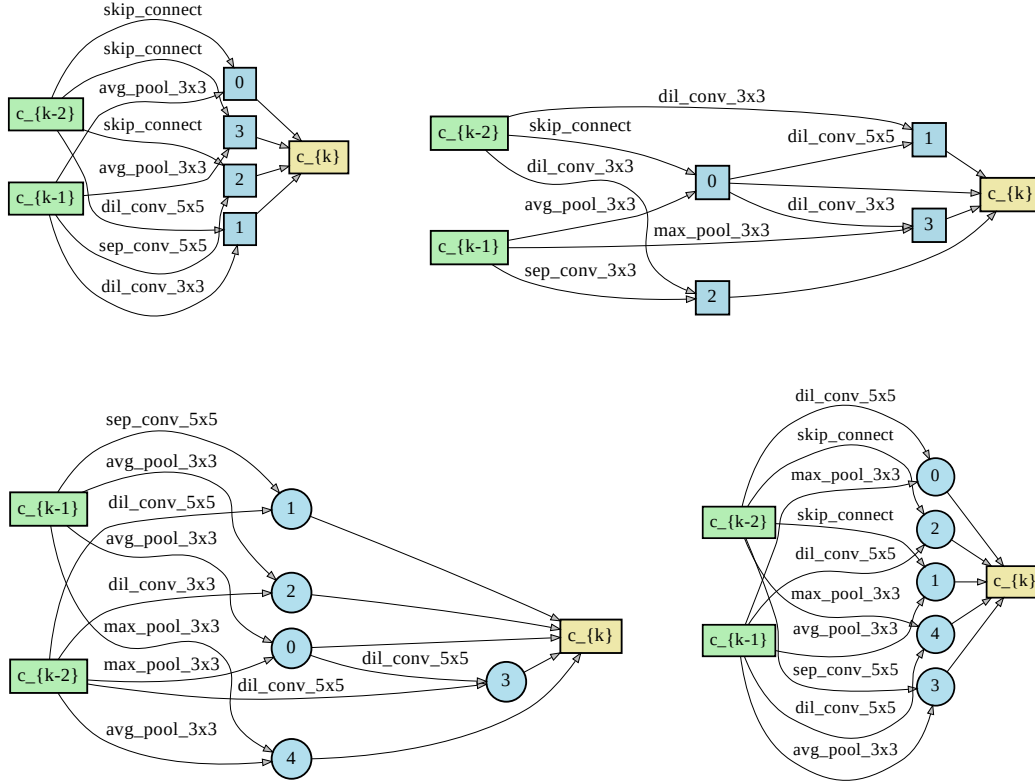


Fig. 7: Cell structures found our proposed approach: Top panel shows discovered normal (left) and reduced (right) cell architectures from search space associated to DermoCSNAS_{N=4}, while bottom panel are associated to DermoCSNAS_{N=5}.

natural discrete search space of NAS problem via SMBO-TPE, enabling competitive/matching results with state-of-the-art algorithms.

There are many directions to conduct further study on CSNAS. For example, computer vision tasks, which involve medical images, are usually considered to lack training samples. This task requires substantially expensive data curation cost, including data gathering and labeling expertise. Another possible CSNAS improvement is investigating further baseline self-supervised learning methods, which potentially ameliorates current CSNAS benchmarks.

ACKNOWLEDGMENTS

Effort sponsored in part by United States Special Operations Command (USSOCOM), under Partnership Intermediary Agreement No. H92222-15-3-0001-01. The U.S. Government is authorized to reproduce and distribute reprints for Government purposes, notwithstanding any copyright notation thereon.¹

REFERENCES

[1] Barret Zoph, Vijay Vasudevan, Jonathon Shlens, and Quoc V Le. Learning transferable architectures for scalable image recognition. In

Proceedings of the IEEE conference on computer vision and pattern recognition, pages 8697–8710, 2018.

[2] Hanxiao Liu, Karen Simonyan, Oriol Vinyals, Chrisantha Fernando, and Koray Kavukcuoglu. Hierarchical representations for efficient architecture search. *arXiv preprint arXiv:1711.00436*, 2017.

[3] Chenxi Liu, Barret Zoph, Maxim Neumann, Jonathon Shlens, Wei Hua, Li-Jia Li, Li Fei-Fei, Alan Yuille, Jonathan Huang, and Kevin Murphy. Progressive neural architecture search. In *Proceedings of the European Conference on Computer Vision (ECCV)*, pages 19–34, 2018.

[4] Esteban Real, Alok Aggarwal, Yanping Huang, and Quoc V Le. Regularized evolution for image classifier architecture search. In *Proceedings of the aaai conference on artificial intelligence*, volume 33, pages 4780–4789, 2019.

[5] Barret Zoph and Quoc V Le. Neural architecture search with reinforcement learning. *arXiv preprint arXiv:1611.01578*, 2016.

[6] Renato Negrinho and Geoff Gordon. Deeparchitect: Automatically designing and training deep architectures. *arXiv preprint arXiv:1704.08792*, 2017.

[7] Kirthevasan Kandasamy, Willie Neiswanger, Jeff Schneider, Barnabas Poczos, and Eric P Xing. Neural architecture search with bayesian optimisation and optimal transport. In *Advances in neural information processing systems*, pages 2016–2025, 2018.

[8] Hanxiao Liu, Karen Simonyan, and Yiming Yang. Darts: Differentiable architecture search. *arXiv preprint arXiv:1806.09055*, 2018.

[9] Yuhui Xu, Lingxi Xie, Xiaopeng Zhang, Xin Chen, Guo-Jun Qi, Qi Tian, and Hongkai Xiong. Pc-darts: Partial channel connections for memory-efficient differentiable architecture search. *arXiv preprint arXiv:1907.05737*, 2019.

[10] Xin Chen, Lingxi Xie, Jun Wu, and Qi Tian. Progressive darts: Bridging the optimization gap for nas in the wild. *International Journal of Computer Vision*, 129(3):638–655, 2021.

[11] Thomas Elsken, Jan-Hendrik Metzen, and Frank Hutter. Simple and efficient architecture search for convolutional neural networks. *arXiv preprint arXiv:1711.04528*, 2017.

[12] Gabriel Bender, Pieter-Jan Kindermans, Barret Zoph, Vijay Vasudevan,

¹The views and conclusions contained herein are those of the authors and should not be interpreted as necessarily representing the official policies or endorsements, either expressed or implied, of the United States Special Operations Command.

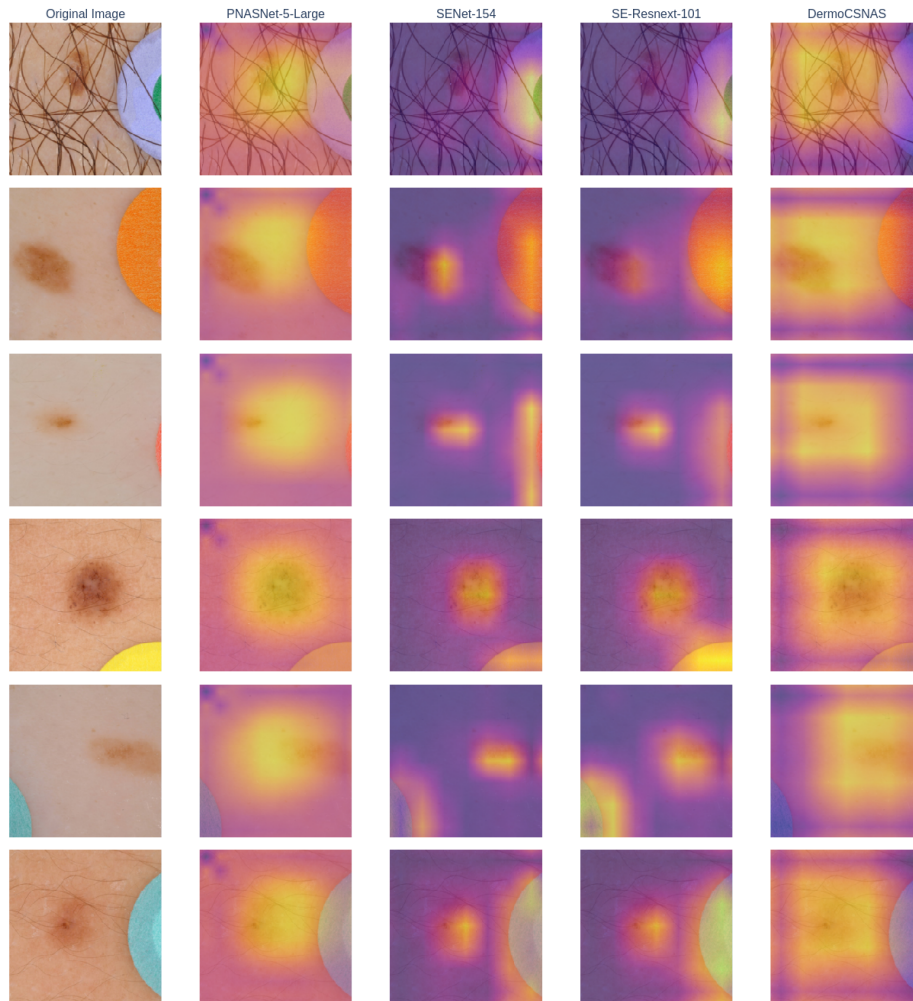


Fig. 8: Classification activation map from noisy test samples, which involve badges and hairs. Searched neural architecture form CSNAS precisely extracts the skin lesion’s regions for classification, while other models partially take badges into account. Furthermore, the sample in the first row shows that our model can correctly locate the skin lesion even though the input image is disturbed by patient’s hairs.

- and Quoc Le. Understanding and simplifying one-shot architecture search. In *International Conference on Machine Learning*, pages 550–559, 2018.
- [13] Hieu Pham, Melody Y Guan, Barret Zoph, Quoc V Le, and Jeff Dean. Efficient neural architecture search via parameter sharing. *arXiv preprint arXiv:1802.03268*, 2018.
- [14] Han Cai, Tianyao Chen, Weinan Zhang, Yong Yu, and Jun Wang. Efficient architecture search by network transformation. In *Thirty-Second AAAI conference on artificial intelligence*, 2018.
- [15] Bowen Baker, Otkrist Gupta, Ramesh Raskar, and Nikhil Naik. Accelerating neural architecture search using performance prediction. *arXiv preprint arXiv:1705.10823*, 2017.
- [16] Andrew Brock, Theodore Lim, James M Ritchie, and Nick Weston. Smash: one-shot model architecture search through hypernetworks. *arXiv preprint arXiv:1708.05344*, 2017.
- [17] Tomas Mikolov, Kai Chen, Greg Corrado, Jeffrey Dean, L Sutskever, and G Zweig. word2vec. URL <https://code.google.com/p/word2vec/>, 22, 2013.
- [18] Armand Joulin, Edouard Grave, Piotr Bojanowski, Matthijs Douze, Herve Jégou, and Tomas Mikolov. Fasttext. zip: Compressing text classification models. *arXiv preprint arXiv:1612.03651*, 2016.
- [19] Jacob Devlin, Ming-Wei Chang, Kenton Lee, and Kristina Toutanova. Bert: Pre-training of deep bidirectional transformers for language understanding. *arXiv preprint arXiv:1810.04805*, 2018.
- [20] Deepak Pathak, Philipp Krahenbuhl, Jeff Donahue, Trevor Darrell, and Alexei A Efros. Context encoders: Feature learning by inpainting. In *Proceedings of the IEEE conference on computer vision and pattern recognition*, pages 2536–2544, 2016.
- [21] Richard Zhang, Phillip Isola, and Alexei A Efros. Split-brain autoencoders: Unsupervised learning by cross-channel prediction. In *Proceedings of the IEEE Conference on Computer Vision and Pattern Recognition*, pages 1058–1067, 2017.
- [22] Alec Radford, Luke Metz, and Soumith Chintala. Unsupervised representation learning with deep convolutional generative adversarial networks. *arXiv preprint arXiv:1511.06434*, 2015.
- [23] Jeff Donahue, Philipp Krähenbühl, and Trevor Darrell. Adversarial feature learning. *arXiv preprint arXiv:1605.09782*, 2016.
- [24] Alexey Dosovitskiy, Philipp Fischer, Jost Tobias Springenberg, Martin Riedmiller, and Thomas Brox. Discriminative unsupervised feature learning with exemplar convolutional neural networks. *IEEE transactions on pattern analysis and machine intelligence*, 38(9):1734–1747, 2015.
- [25] Spyros Gidaris, Praveer Singh, and Nikos Komodakis. Unsupervised representation learning by predicting image rotations. *arXiv preprint arXiv:1803.07728*, 2018.
- [26] Carl Doersch, Abhinav Gupta, and Alexei A Efros. Unsupervised visual representation learning by context prediction. In *Proceedings of the IEEE international conference on computer vision*, pages 1422–1430, 2015.
- [27] Richard Zhang, Phillip Isola, and Alexei A Efros. Colorful image colorization. In *European conference on computer vision*, pages 649–666. Springer, 2016.

- [28] Aaron van den Oord, Yazhe Li, and Oriol Vinyals. Representation learning with contrastive predictive coding. *arXiv preprint arXiv:1807.03748*, 2018.
- [29] Olivier J Hénaff, Aravind Srinivas, Jeffrey De Fauw, Ali Razavi, Carl Doersch, SM Eslami, and Aaron van den Oord. Data-efficient image recognition with contrastive predictive coding. *arXiv preprint arXiv:1905.09272*, 2019.
- [30] Aravind Srinivas, Michael Laskin, and Pieter Abbeel. Curl: Contrastive unsupervised representations for reinforcement learning. *arXiv preprint arXiv:2004.04136*, 2020.
- [31] Jean-Bastien Grill, Florian Strub, Florent Altché, Corentin Tallec, Pierre H Richemond, Elena Buchatskaya, Carl Doersch, Bernardo Avila Pires, Zhaohan Daniel Guo, Mohammad Gheshlaghi Azar, et al. Bootstrap your own latent: A new approach to self-supervised learning. *arXiv preprint arXiv:2006.07733*, 2020.
- [32] Ting Chen, Simon Kornblith, Mohammad Norouzi, and Geoffrey Hinton. A simple framework for contrastive learning of visual representations. *arXiv preprint arXiv:2002.05709*, 2020.
- [33] Ishan Misra and Laurens van der Maaten. Self-supervised learning of pretext-invariant representations. In *Proceedings of the IEEE/CVF Conference on Computer Vision and Pattern Recognition*, pages 6707–6717, 2020.
- [34] Colin Wei, Kendrick Shen, Yining Chen, and Tengyu Ma. Theoretical analysis of self-training with deep networks on unlabeled data. *arXiv preprint arXiv:2010.03622*, 2020.
- [35] Sapir Kaplan and Raja Giryes. Self-supervised neural architecture search. *arXiv preprint arXiv:2007.01500*, 2020.
- [36] Chenxi Liu, Piotr Dollár, Kaiming He, Ross Girshick, Alan Yuille, and Saining Xie. Are labels necessary for neural architecture search? In *European Conference on Computer Vision*, pages 798–813. Springer, 2020.
- [37] Xin Chen, Lingxi Xie, Jun Wu, and Qi Tian. Progressive differentiable architecture search: Bridging the depth gap between search and evaluation. In *Proceedings of the IEEE International Conference on Computer Vision*, pages 1294–1303, 2019.
- [38] Sirui Xie, Hehui Zheng, Chunxiao Liu, and Liang Lin. Snas: stochastic neural architecture search. *arXiv preprint arXiv:1812.09926*, 2018.
- [39] Gao Huang, Zhuang Liu, Laurens Van Der Maaten, and Kilian Q Weinberger. Densely connected convolutional networks. In *Proceedings of the IEEE conference on computer vision and pattern recognition*, pages 4700–4708, 2017.
- [40] Arild Nøkland and Lars Hiller Eidnes. Training neural networks with local error signals. *arXiv preprint arXiv:1901.06656*, 2019.
- [41] Kaiming He, Xiangyu Zhang, Shaoqing Ren, and Jian Sun. Identity mappings in deep residual networks. In *European conference on computer vision*, pages 630–645. Springer, 2016.
- [42] James S Bergstra, Rémi Bardenet, Yoshua Bengio, and Balázs Kégl. Algorithms for hyper-parameter optimization. In *Advances in neural information processing systems*, pages 2546–2554, 2011.
- [43] Alex Krizhevsky, Geoffrey Hinton, et al. Learning multiple layers of features from tiny images. 2009.
- [44] J. Deng, W. Dong, R. Socher, L.-J. Li, K. Li, and L. Fei-Fei. ImageNet: A Large-Scale Hierarchical Image Database. In *CVPR09*, 2009.
- [45] Ting Chen, Yizhou Sun, Yue Shi, and Liangjie Hong. On sampling strategies for neural network-based collaborative filtering. In *Proceedings of the 23rd ACM SIGKDD International Conference on Knowledge Discovery and Data Mining*, pages 767–776, 2017.
- [46] Kaiming He, Haoqi Fan, Yuxin Wu, Saining Xie, and Ross Girshick. Momentum contrast for unsupervised visual representation learning. In *Proceedings of the IEEE/CVF Conference on Computer Vision and Pattern Recognition*, pages 9729–9738, 2020.
- [47] Jia Deng, Wei Dong, Richard Socher, Li-Jia Li, Kai Li, and Li Fei-Fei. Imagenet: A large-scale hierarchical image database. In *2009 IEEE conference on computer vision and pattern recognition*, pages 248–255. Ieee, 2009.
- [48] Zhaohui Yang, Yunhe Wang, Xinghao Chen, Boxin Shi, Chao Xu, Chunjing Xu, Qi Tian, and Chang Xu. Cars: Continuous evolution for efficient neural architecture search. In *Proceedings of the IEEE/CVF Conference on Computer Vision and Pattern Recognition*, pages 1829–1838, 2020.
- [49] Thomas Elsken, Jan Hendrik Metzen, and Frank Hutter. Efficient multi-objective neural architecture search via lamarckian evolution. *arXiv preprint arXiv:1804.09081*, 2018.
- [50] Zhichao Lu, Ian Whalen, Vishnu Boddeti, Yashesh Dhebar, Kalyanmoy Deb, Erik Goodman, and Wolfgang Banzhaf. Nsga-net: neural architecture search using multi-objective genetic algorithm. In *Proceedings of the Genetic and Evolutionary Computation Conference*, pages 419–427, 2019.
- [51] Zhao Zhong, Junjie Yan, Wei Wu, Jing Shao, and Cheng-Lin Liu. Practical block-wise neural network architecture generation. In *Proceedings of the IEEE conference on computer vision and pattern recognition*, pages 2423–2432, 2018.
- [52] Hongpeng Zhou, Minghao Yang, Jun Wang, and Wei Pan. Bayesnas: A bayesian approach for neural architecture search. *arXiv preprint arXiv:1905.04919*, 2019.
- [53] Xuanyi Dong and Yi Yang. Searching for a robust neural architecture in four gpu hours. In *Proceedings of the IEEE/CVF Conference on Computer Vision and Pattern Recognition*, pages 1761–1770, 2019.
- [54] Han Cai, Ligeng Zhu, and Song Han. Proxylessnas: Direct neural architecture search on target task and hardware. *arXiv preprint arXiv:1812.00332*, 2018.
- [55] Chaoyang He, Haishan Ye, Li Shen, and Tong Zhang. Milenas: Efficient neural architecture search via mixed-level reformulation. In *Proceedings of the IEEE/CVF Conference on Computer Vision and Pattern Recognition*, pages 11993–12002, 2020.
- [56] Zhihang Li, Teng Xi, Jiankang Deng, Gang Zhang, Shengzhao Wen, and Ran He. Gp-nas: Gaussian process based neural architecture search. In *Proceedings of the IEEE/CVF Conference on Computer Vision and Pattern Recognition*, pages 11933–11942, 2020.
- [57] Christian Szegedy, Wei Liu, Yangqing Jia, Pierre Sermanet, Scott Reed, Dragomir Anguelov, Dumitru Erhan, Vincent Vanhoucke, and Andrew Rabinovich. Going deeper with convolutions. In *Proceedings of the IEEE conference on computer vision and pattern recognition*, pages 1–9, 2015.
- [58] Sergey Ioffe and Christian Szegedy. Batch normalization: Accelerating deep network training by reducing internal covariate shift. *arXiv preprint arXiv:1502.03167*, 2015.
- [59] Andrew G Howard, Menglong Zhu, Bo Chen, Dmitry Kalenichenko, Weijun Wang, Tobias Weyand, Marco Andreetto, and Hartwig Adam. Mobilenets: Efficient convolutional neural networks for mobile vision applications. *arXiv preprint arXiv:1704.04861*, 2017.
- [60] Xiangyu Zhang, Xinyu Zhou, Mengxiao Lin, and Jian Sun. Shufflenet: An extremely efficient convolutional neural network for mobile devices. In *Proceedings of the IEEE conference on computer vision and pattern recognition*, pages 6848–6856, 2018.
- [61] Ningning Ma, Xiangyu Zhang, Hai-Tao Zheng, and Jian Sun. Shufflenet v2: Practical guidelines for efficient cnn architecture design. In *Proceedings of the European conference on computer vision (ECCV)*, pages 116–131, 2018.
- [62] Jiahui Yu and Thomas Huang. Autoslim: Towards one-shot architecture search for channel numbers. *arXiv preprint arXiv:1903.11728*, 2019.
- [63] Jieru Mei, Yingwei Li, Xiaochen Lian, Xiaojie Jin, Linjie Yang, Alan Yuille, and Jianchao Yang. Atomnas: Fine-grained end-to-end neural architecture search. *arXiv preprint arXiv:1912.09640*, 2019.
- [64] Yingwei Li, Xiaojie Jin, Jieru Mei, Xiaochen Lian, Linjie Yang, Cihang Xie, Qihang Yu, Yuyin Zhou, Song Bai, and Alan L Yuille. Neural architecture search for lightweight non-local networks. In *Proceedings of the IEEE/CVF Conference on Computer Vision and Pattern Recognition*, pages 10297–10306, 2020.
- [65] Dimitrios Stamoulis, Ruizhou Ding, Di Wang, Dimitrios Lymberopoulos, Bodhi Priyantha, Jie Liu, and Diana Marculescu. Single-path nas: Designing hardware-efficient convnets in less than 4 hours. In *Joint European Conference on Machine Learning and Knowledge Discovery in Databases*, pages 481–497. Springer, 2019.
- [66] Mingxing Tan, Bo Chen, Ruoming Pang, Vijay Vasudevan, Mark Sandler, Andrew Howard, and Quoc V Le. Mnasnet: Platform-aware neural architecture search for mobile. In *Proceedings of the IEEE/CVF Conference on Computer Vision and Pattern Recognition*, pages 2820–2828, 2019.
- [67] Francesco Paolo Casale, Jonathan Gordon, and Nicolo Fusi. Probabilistic neural architecture search. *arXiv preprint arXiv:1902.05116*, 2019.
- [68] Bichen Wu, Xiaoliang Dai, Peizhao Zhang, Yanghan Wang, Fei Sun, Yiming Wu, Yuandong Tian, Peter Vajda, Yangqing Jia, and Kurt Keutzer. Fbnet: Hardware-aware efficient convnet design via differentiable neural architecture search. In *Proceedings of the IEEE/CVF Conference on Computer Vision and Pattern Recognition*, pages 10734–10742, 2019.
- [69] Yunyang Xiong, Ronak Mehta, and Vikas Singh. Resource constrained neural network architecture search: Will a submodularity assumption help? In *Proceedings of the IEEE/CVF International Conference on Computer Vision*, pages 1901–1910, 2019.

- [70] Arkadiusz Kwasigroch, Michał Grochowski, and Agnieszka Mikołajczyk. Neural architecture search for skin lesion classification. *IEEE Access*, 8:9061–9071, 2020.
- [71] P Tschandl, C Rosendahl, and H Kittler. The ham10000 dataset, a large collection of multi-source dermatoscopic images of common pigmented skin lesions. *scientific data* 5, 180161 (aug 2018), 2018.
- [72] Noel CF Codella, David Gutman, M Emre Celebi, Brian Helba, Michael A Marchetti, Stephen W Dusza, Aadi Kaloo, Konstantinos Liopyris, Nabin Mishra, Harald Kittler, et al. Skin lesion analysis toward melanoma detection: A challenge at the 2017 international symposium on biomedical imaging (isbi), hosted by the international skin imaging collaboration (isic). In *2018 IEEE 15th International Symposium on Biomedical Imaging (ISBI 2018)*, pages 168–172. IEEE, 2018.
- [73] Marc Combalia, Noel CF Codella, Veronica Rotemberg, Brian Helba, Veronica Vilaplana, Ofer Reiter, Cristina Carrera, Alicia Barreiro, Allan C Halpern, Susana Puig, et al. Bcn20000: Dermoscopic lesions in the wild. *arXiv preprint arXiv:1908.02288*, 2019.
- [74] Terrance DeVries and Graham W Taylor. Improved regularization of convolutional neural networks with cutout. *arXiv preprint arXiv:1708.04552*, 2017.
- [75] Yunpeng Chen, Jianan Li, Huaxin Xiao, Xiaojie Jin, Shuicheng Yan, and Jiashi Feng. Dual path networks. *arXiv preprint arXiv:1707.01629*, 2017.
- [76] Mingxing Tan and Quoc V Le. Efficientnet: Rethinking model scaling for convolutional neural networks. *arXiv preprint arXiv:1905.11946*, 2019.
- [77] Kaiming He, Xiangyu Zhang, Shaoqing Ren, and Jian Sun. Deep residual learning for image recognition. In *Proceedings of the IEEE conference on computer vision and pattern recognition*, pages 770–778, 2016.
- [78] Christian Szegedy, Sergey Ioffe, Vincent Vanhoucke, and Alexander Alemi. Inception-v4, inception-resnet and the impact of residual connections on learning. In *Proceedings of the AAAI Conference on Artificial Intelligence*, volume 31, 2017.
- [79] Jie Hu, Li Shen, and Gang Sun. Squeeze-and-excitation networks. In *Proceedings of the IEEE conference on computer vision and pattern recognition*, pages 7132–7141, 2018.
- [80] François Chollet. Xception: Deep learning with depthwise separable convolutions. In *Proceedings of the IEEE conference on computer vision and pattern recognition*, pages 1251–1258, 2017.

APPENDIX

A. Neural Architecture Search

For CIFAR-10 dataset, we use 5000 class-balanced images to search for the best architecture. While architecture search on ImageNet use the same list of samples as [32].

We use a mini-batch of size $K = 150$, resulting in 298 negative samples corresponding to a single data point each mini-batch. We accelerate the searching time by using small architecture candidates, which include 8 layers and 32 channels. For optimizing the weights w in memory-bank \mathcal{M} , we use momentum SGD with learning rate $\eta_w = 0.001$ and momentum 0.9. We set $\tau = 0.07$ and $\lambda = 0.5$ for the noise contrastive estimator and contrastive loss as in [33]. We set up the TPE sampler as in Sect IV-A with zero initialization for $\theta = (\theta_{\text{normal}}, \theta_{\text{reduce}})$.

B. Neural Architecture Validation

We follow the setup used in [1], [3], [4], [8], where the first and second nodes of cell C_k are set to be compatible to the outputs of cell C_{k-2} and C_{k-1} , respectively. All reduction cells are located in 1/2 and 2/3 of the depth, which has stride two for all operations linked to the input node.

We construct a large network for the CIFAR-10 dataset, including 20 layers with 36 initial channels. The train setting is employed from existing studies [1], [3]–[5], [8], offering

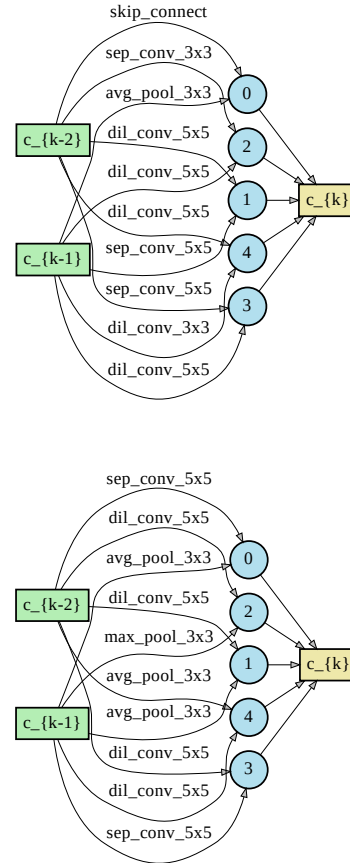


Fig. 9: Cell founded by random search under contrastive self-supervised learning using 10% of CIFAR-10 samples.

more regularization on training, which includes: cutout [74] of length 16, linearly path drop out with probability 0.2 and auxiliary classifier (located in 2/3 maximum depth of the network) with weight 0.4. We train the network for 1200 epochs using batch size 128. The chosen optimizer is momentum SGD with learning rate $\eta = 0.025$, momentum = 0.9, weights decay 3×10^{-4} and gradient clip of 5. The entire training process takes three days on one single GPU.

Regarding the ImageNet dataset, the input resolution is set to be 224×224 , and the allowed number of multiply-add operations is less than 600, which is restricted for mobile settings. We train a network having 14 cells and 48 initial channels for 600 epochs with a batch size of 128. The learning rate is set at $\eta = 0.1$ with decay rate 0.97 and decay period of 2.5. We use the same auxiliary module as the invalidation phase of CIFAR-10. We set the SGD optimizer at a momentum of 0.9, and weights decay 3×10^{-5} .